University of Groningen

Homogeneous Distribution of Magnetic, Antimicrobial-Carrying Nanoparticles through an Infectious Biofilm Enhances Biofilm-Killing Efficacy

Quan, Kecheng; Zhang, Zexin; Ren, Yijin; Busscher, Henk J.; van der Mei, Henny C.; Peterson, Brandon W.

[Link to publication in University of Groningen/UMCG research database](#)

Homogeneous Distribution of Magnetic, Antimicrobial-Carrying Nanoparticles through an Infectious Biofilm Enhances Biofilm-Killing Efficacy
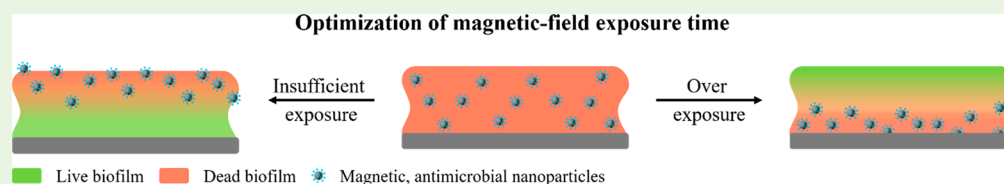
Kecheng Quan,[†,‡] Zexin Zhang,*[,†] Yijin Ren,[§] Henk J. Busscher,*[,‡] Henny C. van der Mei,[‡] and Brandon W. Peterson*[,‡]

†College of Chemistry, Chemical Engineering and Materials Science, Soochow University, Renai road 199, Suzhou 215123, P.R. China

‡Department of Biomedical Engineering, University of Groningen and University Medical Center Groningen, Antonius Deusinglaan 1, 9713 AV Groningen, The Netherlands

§Department of Orthodontics, University of Groningen and University Medical Center Groningen, Hanzeplein 1, 9713 GZ Groningen, The Netherlands

S Supporting Information

Optimization of magnetic-field exposure time

Insufficient exposure — Over exposure

Live biofilm   Dead biofilm   Magnetic, antimicrobial nanoparticles

ABSTRACT: Magnetic, antimicrobial-carrying nanoparticles provide a promising, new and direly needed antimicrobial strategy against infectious bacterial biofilms. Penetration and accumulation of antimicrobials over the thickness of a biofilm is a *conditio sine qua non* for effective killing of biofilm inhabitants. Simplified schematics on magnetic-targeting always picture homogeneous distribution of magnetic, antimicrobial-carrying nanoparticles over the thickness of biofilms, but this is not easy to achieve. Here, gentamicin-carrying magnetic nanoparticles (MNPs-G) were synthesized through gentamicin conjugation with iron-oxide nanoparticles and used to demonstrate the importance of their homogeneous distribution over the thickness of a biofilm. Diameters of MNPs-G were around 60 nm, well below the limit for reticuloendothelial rejection. MNPs-G killed most ESKAPE-panel pathogens, including *Escherichia coli*, equally as well as gentamicin in solution. MNPs-G distribution in a *Staphylococcus aureus* biofilm was dependent on magnetic-field exposure time and most homogeneous after 5 min magnetic-field exposure. Exposure of biofilms to MNPs-G with 5 min magnetic-field exposure yielded not only homogeneous distribution of MNPs-G, but concurrently better staphylococcal killing at all depths than that of MNPs, gentamicin in solution, and MNPs-G, or after other magnet-field exposure times. In summary, homogeneous distribution of gentamicin-carrying magnetic nanoparticles over the thickness of a staphylococcal biofilm was essential for killing biofilm inhabitants and required optimizing of the magnetic-field exposure time. This conclusion is important for further successful development of magnetic, antimicrobial-carrying nanoparticles toward clinical application.

KEYWORDS: magnetic targeting, magnetic nanoparticles, gentamicin, biofilm, infection

Development of new infection-control strategies is becoming more and more urgent. Antimicrobial-resistant bacterial infections have been predicted to become the number one cause of death in the year 2050, exceeding the number of deaths caused by cancer.[1] New infection-control strategies should not only evade rapidly arising bacterial antimicrobial-resistance mechanisms,[2] but preferentially also self-target infectious biofilms and achieve homogeneous distribution of an antimicrobial over the entire thickness of a biofilm. However, such a homogeneous distribution is hard to achieve. Antimicrobials, even when applied to antimicrobial-susceptible strains, solely kill those bacteria that reside on the outer part of a biofilm.[3] As a result, many infections are recurrent, which increases the chances of development of antimicrobial

resistance.[4] Hopes are high that nanotechnology will contribute to the development of new infection-control strategies,[5] for which self-targeting, pH-adaptive antimicrobial micelles, liposomes, or polymersomes, antimicrobial carbon dots and dendrimers, and photothermal and magnetic antimicrobial nanoparticles have all been considered "promising".

Magnetic targeting of drugs is considered promising as a new infection-control strategy and in tumor treatment, as it allows one to establish high drug concentrations at the target
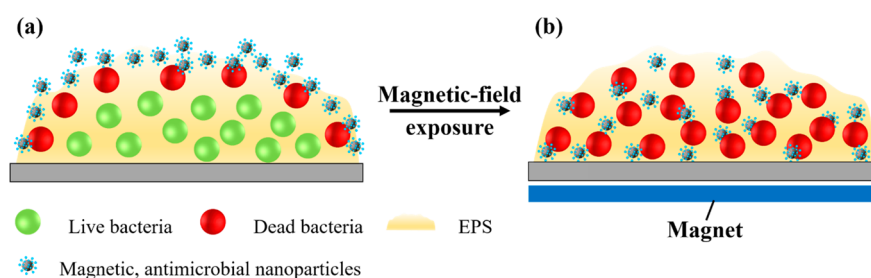
Figure 1. Simplified schematics of magnetic, antimicrobial nanoparticle penetration into an infectious biofilm. (a) The biofilm mode of bacterial growth on a surface prevents penetration of magnetic nanoparticles into an infectious biofilm, and in the absence of a magnetic field magnetic, antimicrobial nanoparticles can solely kill bacteria at the outside of the biofilm. This is the common scenario for antimicrobial penetration in a biofilm.[3] (b) External magnetic fields are frequently pictured to facilitate deep penetration of magnetic nanoparticles into infectious biofilms, while assuming rather than experimentally demonstrating homogeneous distribution of magnetic, antimicrobial nanoparticles across the entire thickness of a biofilm under an applied magnetic-field as trivial.[8−12]

site.[6,7] Magnetic targeting of drugs requires two trivial components: drug-carrying magnetic nanoparticles and a magnet-targeting system. Magnetic targeting of micrometer-sized infections is arguably more difficult, especially *in vivo*, than the targeting of much larger tumors. It is frequently assumed,[8−12] that magnetic, antimicrobial nanoparticles fully penetrate and distribute homogeneously over the thickness of a biofilm under the influence of a magnetic field (see Figure 1). Usually, however, particularly *in vivo*, this is not easy and even targeting of magnetic, antimicrobial nanoparticles to a biofilm site, as opposed to homogeneous distribution over the thickness of a biofilm, requires sophisticated instrumentation.[13]

Current magnetic targeting instrumentation is not suitable to distribute magnetic nanoparticles homogeneously through a biofilm, considering that most clinical biofilms have a thickness limited to 200 μm.[14] A wireless magnetic targeting system has been described for precise control of cylindrical "microrobots" through the posterior segment of the eye for surgical procedures and drug delivery.[15] However, these microrobots had dimensions (1800 × 285 μm^2), exceeding the dimensions of nanoparticles by far. A similar objection holds for the magnetic targeting of nanoparticles as an antimicrobial dispersant of biofilms, requiring nanoparticles with a diameter of 213 nm for targeting,[16] above the critical limit of 200 nm for reticuloendothelial rejection.[17−19]

New technologies for infection-control need to be simple, however, and allow precise control over smaller nanoparticles (<200 nm) over more micrometer-sized dimensions, if downward clinical translation of antimicrobial, magnetically targetable nanoparticles is the goal.[20,21] Also, translation to clinical use will become more likely when new treatment modalities build on conventional ones. Therefore, we recently proposed to use simple, magnetic, non-antimicrobially functionalized nanoparticles to create artificial water channels in infectious biofilms by magnetically induced movement of nanoparticles to make biofilms more penetrable and susceptible to conventional antibiotic treatment.[22] Artificial channel digging does not require any accumulation or precise control or homogeneous distribution of nanoparticles inside the biofilm.

Here, we created magnetic, antimicrobial-carrying nanoparticles, with the aim of demonstrating the difficulty in achieving homogeneous distribution of magnetic, antimicrobial nanoparticles and bacterial killing across the thickness of a biofilm. A simple methodology to achieve homogeneous distribution of magnetic, gentamicin-carrying nanoparticles

across the thickness of an infectious biofilm growing on a biomaterial surface was developed and demonstrated to be accompanied by enhanced killing of biofilm inhabitants. Biomaterial-associated infections are a special class of recalcitrant infections, caused by bacteria forming an infectious biofilm on biomaterials implants and devices, such as total hip or knee arthroplasties, heart valves, vascular grafts, and many other types of implants and devices.[20,23]

First, gentamicin (G), a commonly used aminoglycoside with a wide spectrum of antibacterial activity and particularly suitable for local application,[24] was conjugated through its amino groups to the carboxyl groups on the surface of an iron oxide, magnetic nanoparticle (MNP) using peptide coupling (Figure 2a).[25] Effective conjugation of G to MNPs was demonstrated from the presence of characteristic G- and peptide-coupling bands in Fourier transform infrared (FTIR) spectra (Figure 2b), i.e., the bands at 1400, 1575, and 1650 cm^{-1} due to the stretching of N−H, C−N, and C=O of the peptide coupling and the band at 1030 cm^{-1} attributed to the C−O−C stretching of G. Zeta potentials of MNPs were highly negative (−38.8 ± 2.1 mV; see Figure 2c) due to their carboxyl-rich surface and became positive (8.8 ± 0.2 mV) after G-conjugation[26] as a result of amino-groups in gentamicin. Magnetic properties of MNPs-G (43.4 emu g^{-1}; see Figure 2d) were only slightly lower than those of MNPs (46.8 emu g^{-1}). Thermogravimetric and elemental analysis indicated that G-conjugation in MNPs-G amounted to 24−25% by mass (Figure 2e and f, respectively). The diameter of MNPs-G as obtained using transmission electron microscopy (TEM) was around 60 nm (Figure 2g).

MNPs-G had a broad antibacterial activity against a variety of pathogen members from the so-called ESKAPE-panel,[27] *Enterobacter cloacae* BS 1037, *Staphylococcus aureus* ATCC 12600, *Klebsiella pneumonia*-1, *Acinetobacter baumannii*-1, *Pseudomonas aeruginosa* PA01, and *Enterococcus faecalis* 1396 with the exception of *K. pneumonia* and *A. baumannii* (Figure 3a). In addition to ESKAPE-panel pathogens, MNPs-G were also antibacterially active against *E. coli* ATCC 25922. In general, MBCs of MNPs-G were slightly but significantly lower than of gentamicin. This is likely because electrostatic double-layer attraction between negatively charged bacteria[28] and positively charged MNPs-G demonstrates that conjugation did not negatively impact the antibacterial properties of gentamicin. Growth of mouse fibroblasts with MNPs-G did not negatively impact the metabolic activity of the cells (Figure 3b), while bare magnetic iron oxide nanoparticles were fully
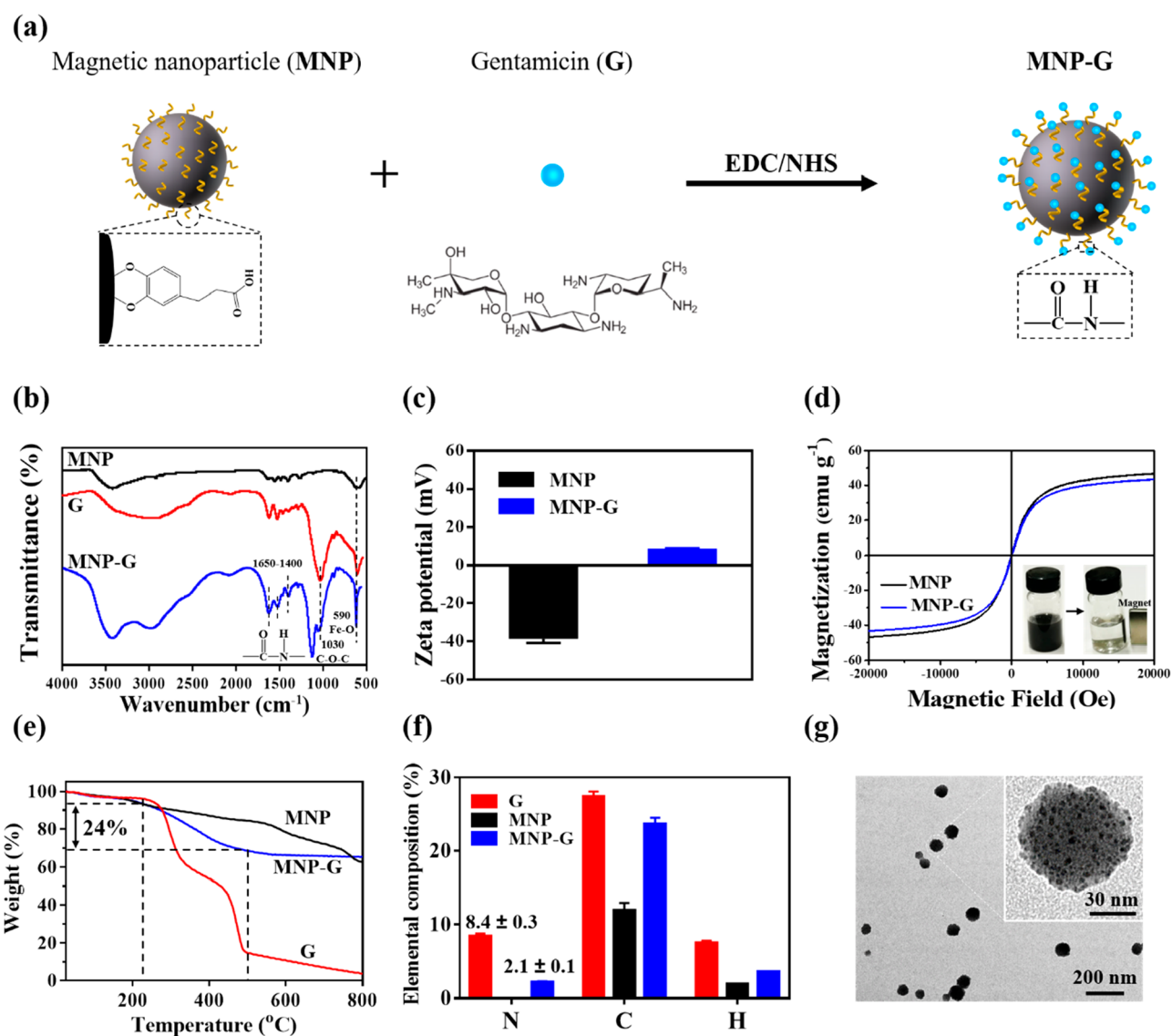
Figure 2. Preparation and characterization of magnetic, gentamicin-carrying nanoparticles (MNPs-G). (a) Synthesis of MNPs-G. The carboxyl (−COOH) group of the carboxyl-functionalized MNP is conjugated with the one of the amino (−NH$_2$) groups on gentamicin through a peptide-coupling, using 1-(3-(dimethylamino)propyl)-3-ethylcarbodiimide hydrochloride (EDC) and N-hydroxy succinimide (NHS) as catalysts. The reaction occurs at room temperature. (b) Fourier transform infrared (FTIR) spectra of G, MNPs, and MNPs-G. (c) Zeta potentials of MNP before and after conjugation of gentamicin in water (pH 7.0). (d) Magnetic hysteresis loops at 300 K for MNPs before and after conjugation of gentamicin, measured by vibrating sample magnetometry. Inset in the lower right corner shows the magnetic behavior of MNPs-G under an applied external magnetic-field. (e) Thermogravimetric analysis of G, MNPs, and MNPs-G. The percent of weight loss over the temperature range between 210 and 490 °C was applied to calculate the weight percent of gentamicin in MNPs-G. (f) Elemental analysis of G, MNPs, and MNPs-G. Nitrogen (N) is absent in MNPs but present in G and MNPs-G, from which it can be concluded that the weight increase of MNPs-G compared to MNPs (panel e) is due to G. Data are expressed as mean ± standard deviation over three separate measurements. (g) TEM micrograph of the MNPs-G as synthesized in this study.

biocompatible with these mammalian cells, as shown previously.[29] This is in line with the known biocompatibility of iron oxide nanoparticles to mammalian cells.[17,30] Moreover, iron oxide nanoparticles are known to be removed from the body through phagocytosis.[31]

Red-fluorescent Rhodamine-B isothiocyanate labeled MNP-G showed a clear depth-dependent distribution of nanoparticles in *S. aureus* biofilms upon magnetic targeting (Figure 4a). After 3 h, upon short magnetic-field exposure (1 and 2 min), nanoparticles accumulated predominantly near the top of the biofilm, while after 5 min an even distribution across the thickness of the biofilm could be observed. Longer magnetic-field exposure times yielded nanoparticle depletion of the

suspension and accumulation of the nanoparticles near the substratum surface, i.e., in the bottom region of the biofilm. In absence of magnetic-field exposure, MNPs-G did not penetrate in the biofilm, and not after prolonged exposure times.

In order to establish a direct relation between MNP-G penetration and staphylococcal killing in biofilms, an identical experiment was carried out in absence of Rhodamine labeling of MNPs-G, but this time staining the bacteria with green-fluorescent SYTO9 and red-fluorescent propidium iodide to distinguish live and dead bacteria, respectively.[10] The number of live (green-fluorescent) and dead (red-fluorescent) bacteria was determined from the confocal laser scanning microscopy (CLSM) images, using ImageJ to quantify the number of
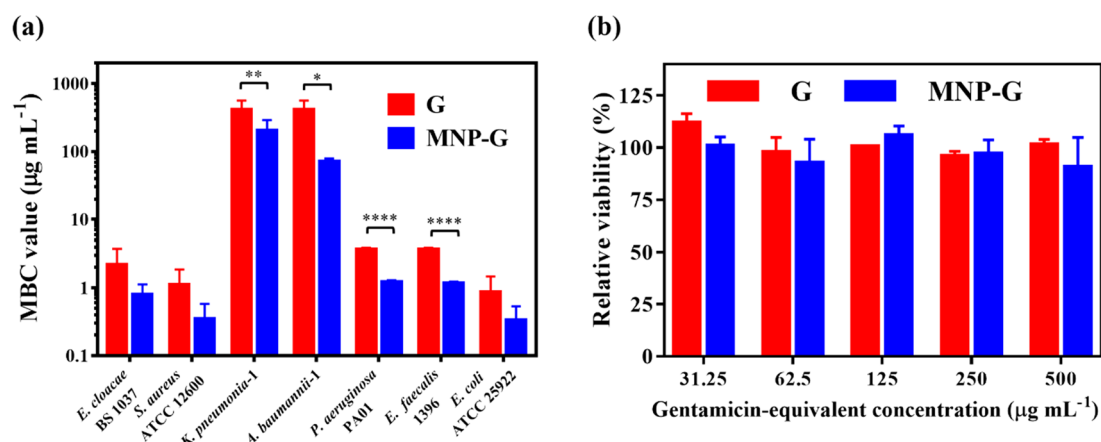
Figure 3. (a) Comparison of the minimal bactericidal concentrations (MBCs) of gentamicin (G) and magnetic nanoparticles with conjugated gentamicin (MNPs-G), expressed in gentamicin-equivalent concentration against ESKAPE pathogens and *E. coli*. Data are expressed as mean ± standard deviation over three separate experiments. Statistical analysis was performed between G and MNPs-G using Student's two-tailed *t* test (**p* < 0.05, ***p* < 0.01, ****p* < 0.0001). (b) Viability of human fibroblasts (American Type Culture Collection ATCC-CRL-2014) after 24 h growth in medium in the presence of different concentrations of G and MNPs-G, as derived from an XTT-conversion assay. Relative viabilities are expressed as mean ± standard deviation over three separate experiments, while 100% represents XTT conversion in PBS.

green- and red-fluorescent bacteria. The distribution of dead bacteria across the thickness of a biofilm roughly followed the same distribution pattern as of MNPs-G (compare Figure 4a and b). Shorter magnetic-field exposure times yielded more dead bacteria near the top of the biofilm, while longer exposure times also caused bacterial death in the bottom of the biofilm. However, the total number of MNPs-G accumulated in a biofilm related well with the number of dead staphylococci over the entire thickness of a biofilm (Figure 4c). This attests to the importance of penetration and homogeneous accumulation of antimicrobial-carrying nanoparticles for killing bacteria in a biofilm mode of growth. Figure 4a and b yields the conclusion that deep killing of biofilm inhabitants requires good penetration of antimicrobial, magnetic nanoparticles in the biofilm (Figure 4b) and that overall killing is highest when antimicrobial nanoparticles distribute homogeneously across the thickness of a biofilm (Figure 4a and b). For the MNPs and magnet setup used here, optimal magnet-exposure time thus equals 5 min.

Finally, using the optimal magnetic-field exposure time of 5 min for deep penetration, killing efficacies of gentamicin, MNPs, and MNPs-G in the absence and presence of magnetic-field exposure were evaluated compared with PBS. MNPs in the presence of magnetic-field exposure yielded a similarly almost no depth-dependence killing (Figure 5a) and low biofilm-killing efficacy (Figure 5b) of *S. aureus* as PBS, while exposure to G or MNPs-G in the absence of magnetic-field exposure yielded low depth-dependent killing and biofilm-killing efficacy. Exposure of staphylococcal biofilms to MNPs-G in the presence of a magnetic-field for the optimal exposure time of 5 min, yielded superior staphylococcal killing at all depths (Figure 5a) and across the entire thickness of the biofilms (Figure 5b).

In conclusion, this work shows that it should not be a priori assumed that magnetic-field exposure yields a homogeneous distribution of magnetic nanoparticles over the entire thickness of a biofilm as is the commonly assumed scenario in the current literature.[8−12] Too short magnetic-field exposure yields accumulation of magnetic nanoparticle near the top of a biofilm, while too long exposure times create more accumulation near the bottom. Under the conditions applied

in this work, homogeneous distribution of magnetic nanoparticles could be achieved using an intermediate magnetic-field exposure time of 5 min, but different culturing platforms, including clinical biofilms, may yield different optimal exposure times. Homogeneous distribution of magnetic, gentamicin-carrying nanoparticles achieved after the optimal magnetic-field exposure time yielded better depth-dependent staphylococcal killing and biofilm-killing efficacy (over an entire biofilm) than other magnetic-field exposure times. Moreover, a homogeneous distribution of magnetic, gentamicin-carrying nanoparticles yielded better killing than gentamicin or magnetic, gentamicin-carrying nanoparticles in absence of magnetic-field exposure. Thus, homogeneous distribution of magnetic, antimicrobial-carrying nanoparticles is a conditio sine qua non for optimal killing. Clinical translation of the use of magnetic, antimicrobial-carrying nanoparticles is not trivial, but it is easiest to achieve for biomaterial-associated infections, in which the bottom of a biofilm is well-defined, as it concurs with the surface of the implant or device (i.e., demonstrated in the current study). In other types of infections, like, e.g., organ infections, a magnetic field might be placed at multiple angles toward an infection site to achieve homogeneous distribution of magnetic, antimicrobial-carrying MNPs in the infectious biofilm, which we demonstrate here is absolutely needed to kill biofilm inhabitants over the depth of a biofilm.

■ EXPERIMENTAL SECTION

Materials. Gentamicin, 3,4-dihydroxyhydrocinnamic acid (DHCA), 1-(3-(dimethylamino)propyl)-3-ethylcarbodiimide hydrochloride (EDC), *N*-hydroxysuccinimide (NHS), 1-octadecene, oleic acid, sodium oleate, and iron(III) chloride ($FeCl_3 \cdot 6H_2O$) were purchased from Aldrich. Tetrahydrofuran (THF), ethanol and hexane were purchased from Sinopharm Chemical Reagent Co. (China). All chemicals were used as received.

Preparation and Characterizations of Magnetic, Gentamicin-Carrying Nanoparticles (MNPs-G). Carboxyl-functionalized, iron oxide magnetic nanoparticles (MNPs, 10 mg mL^{-1}, 1 mL, prepared as described in the Supporting Information) were dispersed in 10 mL of demineralized water (pH 4.0, adjusted by diluted hydrochloric acid) in a 50 mL round-bottom flask. After adding 1 mL of EDC (0.1 M) and 1 mL of NHS (0.1 M), the mixture was stirred for 12 h at room temperature (RT). Then, the pH of the mixture was
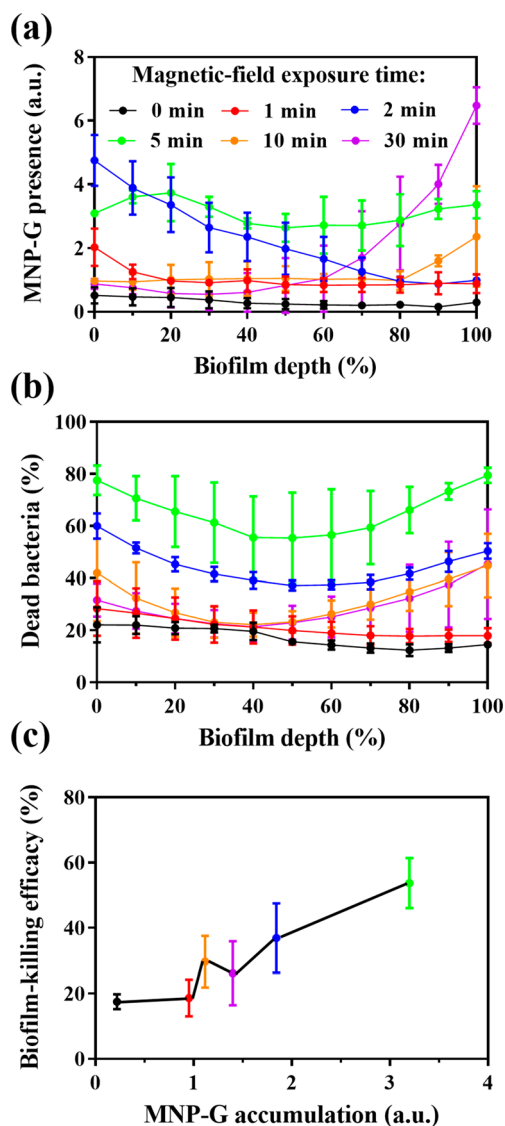
Figure 4. (a) Distribution of Rhodamine-B isothiocyanate labeled MNP-G as a function of the depth in the biofilm (biofilm thicknesses $53 \pm 14 \ \mu$m) for different magnetic-field exposure times, as calculated from CLSM images (see Figure S1a). Biofilms were exposed to MNP-G suspensions in PBS ($440 \ \mu$g mL^{-1}) for 3 h and were made green-fluorescent by staining with SYTO9 in order to distinguish between bacteria and nanoparticles. (b) Percentage of dead bacteria relative to the total number of bacteria in an image stack as a function of depth in the biofilm, as obtained after DEAD/LIVE staining, as calculated from CLSM images (Figure S1b). (c) Bacterial-killing over the entire depth of a biofilm ("biofilm-killing efficacy" relative to the total number of bacteria in a biofilm) as a function of MNPs-G accumulation in a biofilm. Colors correspond with magnetic-field exposure times (see panel a). Data are expressed as mean $\pm$ standard deviation over three separate experiments.

Figure 5. Comparison of the depth-dependent killing of *S. aureus* and biofilm-killing efficacy of *S. aureus* ATCC 12600 upon exposure to gentamicin, MNPs, or MNPs-G in the absence and presence of optimized 5 min magnetic-field exposure. PBS was included as a control. Total exposure time to the antimicrobials was 180 min. (a) Percentage of dead bacteria relative to the total number of bacteria in an image stack as a function of depth in the biofilm, as obtained after DEAD/LIVE staining, as calculated from CLSM images (Figure S2). Superscripts "−" and "+" denote the absence and presence of magnet-field exposure, respectively. (b) Bacterial-killing over the entire depth of a staphylococcal biofilm ("biofilm-killing efficacy" relative to the total number of bacteria in a biofilm). Data are expressed as mean $\pm$ standard deviation over three separate experiments. Statistical analysis was performed using Student's two-tailed *t* test (**$p < 0.01$, ***$p < 0.001$).

adjusted to 9.0 by adding 0.4 mL of NaOH (0.05 M), and 1 mL of gentamicin (0.1 M) was added, followed by stirring for another 12 h at RT. The black particles obtained were magnetically separated and washed with demineralized water three times in order to remove unreacted gentamicin molecules. Finally, MNPs-G were dispersed in phosphate buffered saline (PBS, 5 mM K$_2$HPO$_4$, 5 mM KH$_2$PO$_4$, 150 mM NaCl, pH 7.4) using sonication (Transonic TP 690, ELMA, Germany, 160 W, 35 kHz) at RT for 30 min.

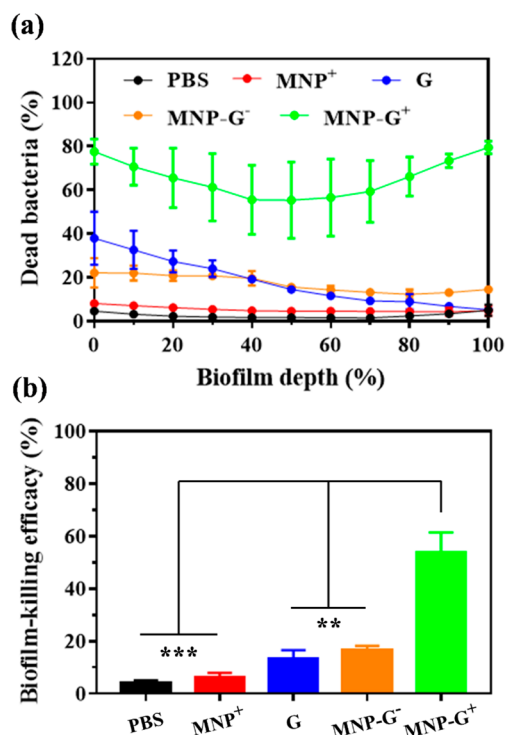The size and shape of MNPs-G were determined using transmission electron microscopy (TEM, G-120, Hitachi, Japan). The conjugation of G to MNP was characterized by Fourier transform infrared spectroscopy (FTIR, Nicolet-20DXB, US). Spectra were taken over a wavenumber range from 500 to 4000 cm^{-1} at a resolution of 2.0 cm^{-1}. All spectra represent averages from 16 interferograms. Zeta potentials were measured in demineralized water using a Malvern NanoSizer ZS2000 (UK). Zeta potentials were measured in triplicate on separately prepared batches of MNPs-G. Magnetic properties of MNPs-G were measured at RT using a vibrating sample magnetometer (model 7410, Lake Shore, USA). The mass content of G in MNPs-G was analyzed using a combination of thermogravimetric (TA2100 USA, heating rate 10 °C min^{-1}) and elemental analysis (Vario EL cube, Germany).

Bacterial Strains, Growth Conditions, and Harvesting. *Enterobacter cloacae* BS 1037, *Staphylococcus aureus* ATCC 12600, *Klebsiella pneumonia*-1, *Acinetobacter baumannii*-1, *Pseudomonas aeruginosa* PA01, *Enterococcus faecalis* 1396, and *Escherichia coli* ATCC 25922 were grown from stock solutions (7% DMSO, kept at −80 °C) on blood agar plates at 37 °C for 24 h. For precultures, a single bacterial colony was transferred into 10 mL of tryptone soy broth (TSB, OXOID, Basingstoke, UK) and incubated 24 h at 37 °C. For main cultures, the preculture was transferred into 200 mL of TSB and incubated for 16 h at 37 °C. Then, bacteria were harvested by centrifugation (5000*g*, 5 min, 10 °C) followed by washing twice in sterile PBS. The bacterial suspension was sonicated (Vibra cell model 375, Sonics and Material Inc., Danbury, CT) three times each for 10 s

with 30 s intervals between each cycle on ice to obtain a suspension with single bacteria. The bacterial concentrations of the suspension were adjusted values appropriate for later use, as determined in a Bürker–Türk counting chamber.

Minimal Bactericidal Concentration (MBC). To determine the MBCs of different strains, 100 μL of G, MNPs, and MNPs-G (1 mg mL^{-1}) in PBS were put in a 96-well plate and 100 μL of TSB was added. Then, solutions were mixed and 2-fold serially diluted. Next, 10 μL of bacterial suspension (1×10^5 bacteria mL^{-1}) was added to mixed solutions in the 96-well plates. After 24 h incubation at 37 °C, 10 μL was taken out of a well and placed on an agar plate and incubated for 24 h at 37 °C. The lowest concentration at which no visible colonies were formed was taken as the MBC value. The experiment was repeated twice with separate bacterial cultures.

MNP-G Distribution in _S. aureus_ Biofilms. For biofilm formation, we selected _S. aureus_ ATCC 12600 for further experiments, as it is a prominent pathogen in many types of infection.[27,32] A staphylococcal suspension (1×10^9 bacteria mL^{-1}, 2 mL) was put into a sterile polystyrene 12-well plate for 2 h at RT in order to allow bacterial adhesion. Thereafter, the suspension was removed, and the well was washed three times with sterile PBS, filled with fresh TSB, and incubated for 24 h at 37 °C.

In order to visualize depth-dependent distribution of MNPs-G after penetration and accumulation in staphylococcal biofilms, MNPs-G were first labeled with red-fluorescent Rhodamine-B isothiocyanate (Sigma-Aldrich, USA). To this end, 10 mg of MNP-G and 1 mg of Rhodamine-B isothiocyanate were mixed in 10 mL of PBS and stirred for 8 h in the dark at RT. Then, the suspension was dialyzed for 48 h in demineralized water to remove unreacted Rhodamine-B isothiocyanate, while refreshing the water every 12 h. After dialysis, the Rhodamine-B isothiocyanate labeled MNPs-G were magnetically separated and resuspended in PBS for later use. Next, 24 h _S. aureus_ biofilms were washed once with sterile PBS, exposed to 2 mL of red-fluorescent MNP-G (440 μg mL^{-1}) under a magnetic-field created by a NdFeB magnet (1 mm thickness and 10 mm in diameter with 1.17–1.21 T residual magnetism) for different times (0, 1, 2, 5, 10, and 30 min) at 37 °C. After magnetic-field exposure, biofilms were placed in the incubator again. The total exposure time of the biofilms to MNPs-G amounted to 180 min, including magnetic-field exposure and incubation. After incubation, the nanoparticle suspension was removed and bacteria in the biofilms were stained with green-fluorescent SYTO9 (Thermo Fisher Scientific, Waltham, MA) for 15 min at RT in the dark. Finally, biofilms were washed once with PBS and subsequently imaged by CLSM (Leica TCS SP2 Leica, Wetzlar, Germany) with an HCX APO L40×/0.80 W U-V-1 objective. An argon ion laser at 488 nm and a green HeNe laser at 543 nm were used to excite the SYTO9 and Rhodamine-B isothiocyanate, and fluorescence was collected at 500–540 nm (SYTO9) and 583–688 nm (Rhodamine-B isothiocyanate). CLSM images were acquired using Leica software, version 2.0.

The presence of Rhodamine-B isothiocyanate labeled MNPs-G in each image stack of a biofilm or in an entire biofilm ("MNPs-G accumulation") was calculated as the ratio of red-fluorescent over green-fluorescent pixels, either in an image stack or in an entire biofilm. The distribution of MNPs-G across the thickness of staphylococcal biofilms was measured in triplicate, using separate bacterial cultures.

S. aureus Killing in Biofilms. Twenty-four hour _S. aureus_ biofilms were exposed to MNPs-G (no Rhodamine-B isothiocyanate labeling). Afterward, they were stained with green-fluorescent SYTO9 and red-fluorescent propidium iodide (Thermo Fisher Scientific, Waltham, MA) for 15 min at RT in the dark to label live and dead bacteria, respectively, in the biofilm. Biofilms were subsequently imaged by CLSM, and depth-dependent staphylococcal killing or killing over the entire thickness of a biofilm ("biofilm killing efficacy") was calculated using ImageJ as the percentage red-fluorescent over the sum of red- and green-fluorescent pixels, either in an image stack or in an entire biofilm, respectively.

In order to compare the biofilm-killing efficacy of MNPs-G after optimized magnetic-field exposure, 24 h staphylococcal biofilms were exposed to PBS, G (110 μg mL^{-1} in PBS, equivalent concentration as in MNPs-G), MNPs-G or MNPs (440 μg mL^{-1}, in PBS) with magnetic-field exposure, and MNP-G (440 μg mL^{-1} in PBS) with and without magnetic-field for 5 min, while total exposure time to antimicrobials was 180 min, including magnetic-field exposure and incubation. The experiment was repeated in triplicate with separate staphylococcal cultures.

Effects of MNPs-G on Mammalian Cells. The cytotoxicity of MNP-G and G was evaluated according to a previous method.[22] Briefly, human fibroblasts (American Type Culture Collection ATCC-CRL-2014) were cultured in 96-well plates (5×10^3 cells per well), filled with 100 μL of cell growth medium (Dulbecco's modified Eagle's medium (DMEM, ThermoFisher Scientific) supplemented with 10% fetal bovine serum (FBS; Invitrogen)). Subsequently, 100 μL of MNPs-G or G in cellular growth medium (concentration range 31.25–500 μg mL^{-1} in G-weight equivalents) was added and incubated for 24 h in 5% CO_2 at 37 °C. After 24 h, 50 μL of XTT ((2,3-bis(2-methoxy-4-nitro-5-sulfophenyl)-2H-tetrazo-lium-5-carboxanilide salt), AppliChem) reagent solution combined with activation solution (PMS, N-methyl dibenzopyrazine methyl sulfate, Sigma-Aldrich) was added. After another 4 h at 37 °C, absorbances A_{485nm} were measured using a spectrophotometer (Shimadzu, Japan). According to the manufacturer's instructions, A_{690nm} was measured and subtracted as a reference control. The viability of the fibroblasts after material exposure was calculated relative to the one of cells exposed to PBS in the absence of material according to

$$\text{relative viability (\%)} = \frac{A_{\text{material485nm}} - A_{\text{material690nm}}}{A_{\text{PBS485nm}} - A_{\text{PBS690nm}}} \times 100\%$$

(1)

Statistics. All comparisons of MBCs and biofilm-killing efficacies between the different treatments were performed with a two-tailed Student's _t_ test, accepting significance at $p < 0.05$.

■ ASSOCIATED CONTENT

Ⓢ Supporting Information

The Supporting Information is available free of charge at https://pubs.acs.org/doi/10.1021/acsbiomaterials.9b01425.

> Detailed synthesis of magnetic, carboxyl-functionalized iron oxide nanoparticles; representative 3D-CLSM images of _S. aureus_ ATCC 12600 biofilms exposed to Rhodamine-B isothiocyanate labeled MNPs-G and LIVE/DEAD staining; representative 3D-CLSM images of _S. aureus_ ATCC 12600 biofilms exposed to different treatments with optimized magnetic exposure time (PDF)

■ AUTHOR INFORMATION

Corresponding Authors

*(Z.Z.) Email: zhangzx@suda.edu.cn. Telephone: +8651269155295.
*(H.J.B.) Email: h.j.busscher@umcg.nl. Telephone: +31503616094.
*(B.W.P.) Email: b.w.peterson@umcg.nl. Telephone: +31503616110.

ORCID Ⓘ

Zexin Zhang: 0000-0002-4963-5002
Henny C. van der Mei: 0000-0003-0760-8900
Brandon W. Peterson: 0000-0002-8969-3696

Notes

Opinions and assertions contained herein are those of the authors and are not construed as necessarily representing views of their respective employers.

The authors declare the following competing financial interest(s): H.J.B. is also director of a consulting company, SASA BV (GN Schutterlaan 4, 9797 PC Thesinge, The Netherlands). The authors declare no potential conflicts of interest with respect to authorship and/or publication of this article.

■ REFERENCES

(1) Humphreys, G.; Fleck, F. United Nations Meeting on Antimicrobial Resistance. *Bull. World Health Organ.* **2016**, *94*, 638–639.

(2) Simoes, M.; Simoes, L. C.; Vieira, M. J. A Review of Current and Emergent Biofilm Control Strategies. *LWT-Food Sci. Technol.* **2010**, *43*, 573–583.

(3) Davies, D. Understanding Biofilm Resistance to Antibacterial Agents. *Nat. Rev. Drug Discovery* **2003**, *2*, 114–122.

(4) de la Fuente-Nunez, C.; Reffuveille, F.; Fernandez, L.; Hancock, R. E. W. Bacterial Biofilm Development as a Multicellular Adaptation: Antibiotic Resistance and New Therapeutic strategies. *Curr. Opin. Microbiol.* **2013**, *16*, 580–589.

(5) Liu, Y.; Shi, L.; Su, L.; van der Mei, H. C.; Jutte, P. C.; Ren, Y.; Busscher, H. J. Nanotechnology-based Antimicrobials and Delivery Systems for Biofilm-infection Control. *Chem. Soc. Rev.* **2019**, *48*, 428–446.

(6) Hajipour, M. J.; Fromm, K. M.; Ashkarran, A.; Aberasturi, D.; Larramendi, L.; Rojo, T.; Serpooshan, V.; Parak, W. J.; Mahmoudi, M. Antibacterial Properties of Nanoparticles. *Trends Biotechnol.* **2012**, *30*, 499–511.

(7) Ulbrich, K.; Hola, K.; Subr, V.; Bakandritsos, A.; Tucek, J.; Zboril, R. Targeted Drug Delivery with Polymers and Magnetic Nanoparticles: Covalent and Noncovalent Approaches, Release Control, and Clinical Studies. *Chem. Rev.* **2016**, *116*, 5338–5431.

(8) Subbiahdoss, G.; Sharifi, S.; Grijpma, D. W.; Laurent, S.; Van der Mei, H. C.; Mahmoudi, M.; Busscher, H. J. Magnetic Targeting of Surface-modified Superparamagnetic Iron Oxide Nanoparticles Yields Antibacterial Efficacy Against Biofilms of Gentamicin-Resistant Staphylococci. *Acta Biomater.* **2012**, *8*, 2047–2055.

(9) Geilich, B. M.; Gelfat, L.; Sridhar, S.; Van de Ven, A. L.; Webster, T. J. Superparamagnetic Iron Oxide-encapsulating Polymersome Nanocarriers for Biofilm Eradication. *Biomaterials* **2017**, *119*, 78–85.

(10) Wang, X.; Deng, A.; Cao, W.; Li, Q.; Wang, L.; Zhou, J.; Hu, B.; Xing, X. Synthesis of Chitosan/Poly (Ethylene Glycol)-modified Magnetic Nanoparticles for Antibiotic Delivery and Their Enhanced Anti-biofilm Activity in the Presence of Magnetic Field. *J. Mater. Sci.* **2018**, *53*, 6433–6449.

(11) Wang, X.; Wu, J.; Li, P.; Wang, L.; Zhou, J.; Zhang, G.; Li, X.; Hu, B.; Xing, X. Microenvironment-Responsive Magnetic Nanocomposites Based on Silver Nanoparticles/Gentamicin for Enhanced Biofilm Disruption by Magnetic Field. *ACS Appl. Mater. Interfaces* **2018**, *10*, 34905–34915.

(12) Zhang, C.; Du, C.; Liao, J.; Gu, Y.; Gong, Y.; Pei, J.; Gu, H.; Yin, D.; Gao, L.; Pan, Y. Synthesis of Magnetite Hybrid Nanocomplexes to Eliminate Bacteria and Enhance Biofilm Disruption. *Biomater. Sci.* **2019**, *7*, 2833–2840.

(13) Shapiro, B.; Kulkarni, S.; Nacev, A.; Sarwar, A.; Preciado, D.; Depireux, D. A. Shaping Magnetic Fields to Direct Therapy to Ears and Eyes. *Annu. Rev. Biomed. Eng.* **2014**, *16*, 455–481.

(14) Bjarnsholt, T.; Alhede, M.; Alhede, M.; Eickhardt-Sorensen, S. R.; Moser, C.; Kuhl, M.; Jensen, P.; Hoiby, N. The In Vivo Biofilm. *Trends Microbiol.* **2013**, *21*, 466–474.

(15) Ullrich, F.; Bergeles, C.; Pokki, J.; Ergeneman, O.; Erni, S.; Chatzipirpiridis, G.; Pane, S.; Framme, C.; Nelson, B. J. Mobility Experiments with Microrobots for Minimally Invasive Intraocular Surgery. *Invest. Ophthalmol. Visual Sci.* **2013**, *54*, 2853–2863.

(16) Hwang, G.; Paula, A. J.; Hunter, E. E.; Liu, Y.; Babeer, A.; Karabucak, B.; Stebe, K.; Kumar, V.; Steager, E.; Koo, H. Catalytic Antimicrobial Robots for Biofilm Eradication. *Science Robotics* **2019**, *4*, No. eaaw2388.

(17) Gupta, A. K.; Gupta, M. Synthesis and Surface Engineering of Iron Oxide Nanoparticles for Biomedial Applications. *Biomaterials* **2005**, *26*, 3995–4021.

(18) Moghimi, S. M.; Hunter, A. C.; Murray, J. C. Long-Circulating and Target-Specific Nanoparticles: Theory to Practice. *Pharmacol. Rev.* **2001**, *53*, 283–318.

(19) Petros, R. A.; DeSimone, J. M. Strategies in the Design of Nanoparticles for Therapeutic Applications. *Nat. Rev. Drug Discovery* **2010**, *9*, 615–627.

(20) Busscher, H. J.; Van der Mei, H. C.; Subbiahdoss, G.; Jutte, P. C.; Van den Dungen, J. J. A. M.; Zaat, S. A. J.; Schultz, M. J.; Grainger, D. W. Biomaterial-Associated Infection: Locating the Finish Line in the Race for the Surface. *Sci. Transl. Med.* **2012**, *4*, 153rv10.

(21) Busscher, H. J.; Alt, V.; Van der Mei, H. C.; Fagette, P. H.; Zimmerli, W.; Moriarty, T. F.; Parvizi, J.; Schmidmaier, G.; Raschke, M. J.; Gehrke, T.; Bayston, R.; Baddour, L. M.; Winterton, L. C.; Darouiche, R. O.; Grainger, D. W. A Trans-atlantic Perspective on Stagnation in Clinical Translation of Antimicrobial Strategies for the Control of Biomaterial-implant Associated Infection. *ACS Biomater. Sci. Eng.* **2019**, *5*, 402–406.

(22) Quan, K.; Zhang, Z.; Chen, H.; Ren, X.; Ren, Y.; Peterson, B. W.; Van der Mei, H. C.; Busscher, H. J. Artificial Channels in an Infectious Biofilm Created by Magnetic Nanoparticles Enhance Bacterial Killing by Antibiotics. *Small* **2019**, *15*, 1902313.

(23) Arciola, C. R.; Campoccia, D.; Montanaro, L. Implant Infections: Adhesion, Biofilm Formation and Immune Evasion. *Nat. Rev. Microbiol.* **2018**, *16*, 397–409.

(24) Lucke, M.; Schmidmaier, G.; Sadoni, S.; Wildemann, B.; Schiller, R.; Haas, N. P.; Raschke, M. Gentamicin Coating of Metallic Implants Reduces Implant-Related Osteomyelitis in Rats. *Bone* **2003**, *32*, 521–531.

(25) Loomans, E. E. M. G.; van Wiltenburg, J.; Koets, M.; van Amerongen, A. Neamin as an Immunogen for the Development of a Generic ELISA Detecting Gentamicin, Kanamycin, and Neomycin in Milk. *J. Agric. Food Chem.* **2003**, *51*, 587–593.

(26) Pothayee, N.; Pothayee, N.; Jain, N.; Hu, N.; Balasubramaniam, S.; Johnson, L. M.; Davis, R. M.; Sriranganathan, N.; Riffle, J. S. Magnetic Block Ionomer Complexes for Potential Dual Imaging and Therapeutic Agents. *Chem. Mater.* **2012**, *24*, 2056–2063.

(27) Pendleton, J. N.; Gorman, S. P.; Gilmore, B. F. Clinical Relevance of the ESKAPE Pathogens. *Expert Rev. Anti-Infect. Ther.* **2013**, *11*, 297–308.

(28) Bayer, M. E.; Sloyer, J. L. The Electrophoretic Mobility of Gram-negative and Gram-positive Bacteria: an Electrokinetic Analysis. *J. Gen. Microbiol.* **1990**, *136*, 867–874.

(29) Dai, R.; Hang, Y.; liu, Q.; Zhang, S.; Wang, L.; Pan, Y.; Chen, H. Improved Neural Differentiation of Stem Cells Mediated by Magnetic Nanoparticle-Based Biophysical Stimulation. *J. Mater. Chem. B* **2019**, *7*, 4161–4168.

(30) Mahmoudi, M.; Simchi, A.; Imani, M.; Shokrgozar, M. A.; Milani, A. S.; Hafeli, U. O.; Stroeve, P. A New Approach for the In Vitro Identification of the Cytotoxicity of Superparamagnetic Iron Oxide Nanoparticles. *Colloids Surf., B* **2010**, *75*, 300–309.

(31) Yu, Q.; Xiong, X.; Zhao, L.; Xu, T.-T.; Bi, H.; Fu, R.; Wang, Q.-H. Biodistribution and Toxicity Assessment of Superparamagnetic Iron Oxide Nanoparticles In Vitro and In Vivo. *Curr. Med. Sci.* **2018**, *38*, 1096–1102.

(32) Lowy, F. D. *Staphylococcus aureus* Infections. *N. Engl. J. Med.* **1998**, *339*, 520−532.